Structure and Photoluminescence Study of TiO_2 Nanoneedle Texture along Vertically Aligned Carbon Nanofiber Arrays

Jianwei Liu,[†] Jun Li,*[,†] Ashok Sedhain,[‡] Jingyu Lin,[‡] and Hongxing Jiang[‡]

Department of Chemistry, Kansas State University, Manhattan, Kansas 66506-3701, and Department of Physics, Kansas State University, Manhattan, Kansas 66506-2601

Received: July 09, 2008; Revised Manuscript Received: September 01, 2008

A hybrid TiO_2−carbon nanofiber hierarchical nanostructure has been fabricated by the metal−organic chemical vapor deposition of a TiO_2 layer onto the vertically aligned carbon nanofiber array. As the deposition time increases from 10 to 60 min, the TiO_2 coating changes from the particulated conformal ultrathin film to a nanoneedle-like texture along the sidewall of the carbon nanofibers. X-ray diffraction indicates that the TiO_2 form anatase crystals with the coherent length over 50 nm, in good agreement with transmission electron microscopy images. Photoluminescence spectra are taken at both room temperature and 10 K. The absence of photoluminescence emission indicates that the electron−hole recombination in TiO_2 is completely quenched in such core−shell hybrid structure. The charge separation may be much more effective at the TiO_2−carbon nanofiber heterojunction. The nanoneedle-like texture drastically increases the effective surface area of the TiO_2 while maintaining a much more effective electrical wiring through the highly conductive carbon nanofiber core. Such hierarchical architecture may be used as a novel anode material for dye-sensitized solar cells.

Introduction

Inspired by natural photosynthesis, dye-sensitized solar cell (DSC) has been developed to convert the photo energy into electricity.[1] At the heart of the device is a mesoporous oxide layer composed of a network of TiO_2 nanoparticles (NPs), which have been sintered together to establish electronic conduction. The nanostructured TiO_2 network is used as a scaffold to hold a large number of dye molecules to increase photon absorption in a given geometric area of the DSC. However, the electron transport rate in such random TiO_2 NP network is strongly influenced by the density of interconnected electron pathway. To improve the electron transport and decrease the electron trap due to recombination with oxidized sensitizers at the NP surface, oriented TiO_2 nanotube (NT) arrays,[2,3] ZnO nanowires (NWs) with a branched structure,[4] and an array of oriented single-crystalline ZnO NWs[5] have been employed to replace the NP film as anodes in DSCs. Electron transport in crystalline NWs is expected to be several orders of magnitude faster than percolation through a random polycrystalline network. The direct electronic pathways provided by the NWs ensure the rapid collection of charge carriers generated throughout the device,[5] which is particularly promising for future DSCs. However, the energy conversion efficiency of these NW-based DSCs (1.5−2.5%) is significantly lower than the traditional DSCs[6] (7.1−10.4%), presumably due to the smaller surface area of semiconductor materials (only ∼1/5 of that of TiO_2 NP film in traditional DSCs).[5]

On the other hand, the intrinsic electrical properties of semiconductor NWs as an electron pathway need to be re-examined. A ZnO NW with 50 nm diameter and 5 μm length was measured with a resistance of 1−3.5 MΩ,[5,7] which is far from a good ohmic connetion. Vertically aligned carbon nanofibers (VACNFs), a variant of aligned multiwalled carbon nanotubes (MWCNTs) grown by plasma enhanced chemical vapor deposition (PECVD), have shown perfect linear $I-V$ characteristics with a resistance of less than 10 kΩ at the same dimension (corresponding to a resistivity $\rho = (4-7) \times 10^{-4}$ Ω-cm) using two-terminal measurements from the ends of CNFs.[8,9] This is close to the value using four-probe side-contact measurements on individual CNFs ($\rho = (3-7) \times 10^{-3}$ Ω-cm).[10] A recent paper demonstrated that needle-like metal structures with higher electrically active surface area can be electroless deposited on VACNFs.[11] It would be very interesting to deposit TiO_2 with similar structures for DSCs. In addition, CNFs have a work function similar to that of MWCNTs,[12] matching that of transparent indium−tin-oxide (ITO) electrodes.[13] Thus, CNFs and CNTs can serve as ideal electron pathways to collect electrons from photoexcited dye molecules. The superior vertical alignment and strong mechanical properties of VACNFs also make them an ideal nanostructured template to support a thin TiO_2 coating that is required as a barrier for electron−hole separation. Here, we demonstrate the formation of such a hybrid TiO_2−VACNF hierarchical nanostructure by the metal−organic chemical vapor deposition (MOCVD) of TiO_2 onto VACNF templates. Interestingly, after sufficient deposition, TiO_2 forms a nanoneedle-like texture with greatly enhanced surface area. Such a hierarchical architecture is expected to improve both the TiO_2 surface area and the efficiency of electron collection in DSCs.

The potential in enhancing the capture and transport of photogenerated electrons through highly conductive long CNTs has been explored in a few recent studies. Konkanand et al.[14] demonstrated that TiO_2 NPs dispersed on single-walled carbon nanotube (SWCNT) network scaffolds could boost the photo-conversion efficiency of a photoelectrochemical cell by a factor of 2. Yu et al.[15] have reported the deposition of TiO_2 NPs on aligned MWCNTs grown on a Ti foil. The photoelectrochemical studies indicated that the TiO_2−MWCNT heterojunction could minimize the recombination of photoinduced electrons and

* Corresponding author. Phone: (785) 532-0955. E-mail: junli@ksu.edu.
[†] Department of Chemistry.
[‡] Department of Physics.

10.1021/jp8060653 CCC: $40.75
Published on Web 10/10/2008

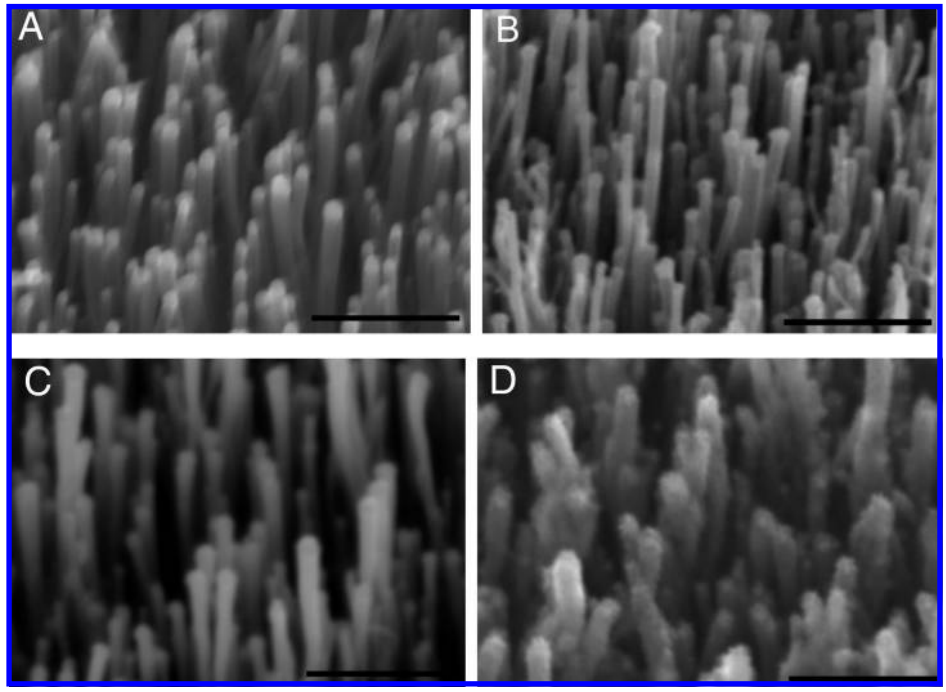

Figure 1. SEM images of (A) an as-grown VACNF array, and (B), (C), (D) the VACNF arrays after coating TiO_2 for 10, 30, and 60 min via MOCVD, respectively. All scale bars are 2 μm.

holes, generating a short circuit photocurrent 5 times more than that of the aligned TiO_2 nanotubes on Ti substrates.

Clearly, the conversion efficiency of DSCs can be improved if we further increase the surface area of the scaffolds and improve photoinduced charge separation and carrier transport by the introduction of a better TiO_2−CNT heterojunction at the anode. Here, we report on the fabrication of a hybrid TiO_2−VACNF architecture, where individual freestanding VACNF arrays serve both as the support for the three-dimensional (3-D) core−shell structure during the metal−organic chemical vapor deposition (MOCVD) and as a conductor connecting the photovoltaic materials. The TiO_2 coating on VACNFs can suppress recombination by introducing an energy barrier that increases the physical separation between photoinjected electrons and the oxidized redox species (holes) in the electrolyte, and forming a tunneling barrier that corrals electrons within the conducting cores or passivating recombination centers on the oxide surface.[16] The 300−400 nm spacing between CNFs makes it feasible for the vapor precursors to access the whole CNF surface and form a uniform coating all of the way down to the bottom. With enough deposition, TiO_2 forms nanoneedle texture along the sidewall of CNFs. An analysis of the photoluminescence spectra indicates the fluorescence quenching due to electron−hole separation at the TiO_2−CNF heterojunction.

Experimental Methods

There are four steps in this study. First, a VACNF array was grown from the Ni catalyst-coated Si substrate using a home-built DC biased PECVD system.[17,18] Second, TiO_2 layer was deposited on the VACNF via MOCVD using a tube furnace (Lindberg/Blue, EW-33850) directly supplied with titanium isopropoxide vapor, $[Ti\{OCH(CH_3)_2\}_4]$ (ACROS, ORGANICS, 98%), under 150 mTorr at 550 °C for 10−60 min. Third, the structure of the hybrid TiO_2−VACNF arrays was characterized with scanning electron microscopy (SEM) (Hitachchi S-3400 N) and X-ray diffraction (XRD) as intact vertical arrays on Si substrates. XRD was performed with a Bruker D8 X-ray diffractometer with the monochrochromatic Cu Kα radiation ($\lambda = 1.542$ Å). Some TiO_2-coated CNFs were scraped off from the Si substrate and deposited on a grid for transmission electron microscopy (TEM) measurements using FEI CM100 with accelerating voltages up to 100 kV. Finally, the optical properties of the hybrid TiO_2−VACNF array and its charge separation capability were probed by continuous-wave (cw) photoluminescence (PL) emission spectroscopy. The excitation pulses of about 100 fs at a repetition rate of 76 MHz were generated by a frequency tripled Ti-sapphire laser with an average power of 50 mW at 263 nm (4.71 eV). A single-photon counting detection system together with a microchannel-plate photomultiplier tube and a 1.3 m monochromator has the detection capability ranging from 185 to 800 nm. Low temperature (10 K) PL measurements were performed by mounting the sample in a stage with a coldfinger in a closed-cycle helium refrigerator. Commercial anatase TiO_2 NP with the diameter of ~15 nm (MKnano, MKN-TiO_2-015A) was used as a reference sample in XRD and PL measurements.

Results and Discussion

Figure 1A shows a SEM image of an as-growth VACNF array, revealing that each CNF is well aligned vertically at the substrate surface and separated from its neighbors. The average diameter of the CNF is ca. 80 nm in this sample, and the length is about 5 μm. A more detailed investigation of as-grown CNF by TEM (Figure 2A) demonstrated that the CNFs have a mean diameter of ca. 80 nm, consistent with the SEM observation. From the TEM image, we can see bamboo-like closed graphitic shells across the hollow central channel along the tube axis, which is due to the fact that the graphitic layers are not perfectly parallel to the tube axis. The Ni catalyst particles remain at the tip enclosed with a few graphitic carbon layers as reported before.[17,18] This structure is a representative signature resulted from the PECVD growth processes and thus is commonly referred to as CNFs to be structurally distinguished from MWCNTs. Figure 1A shows a large space between neighboring

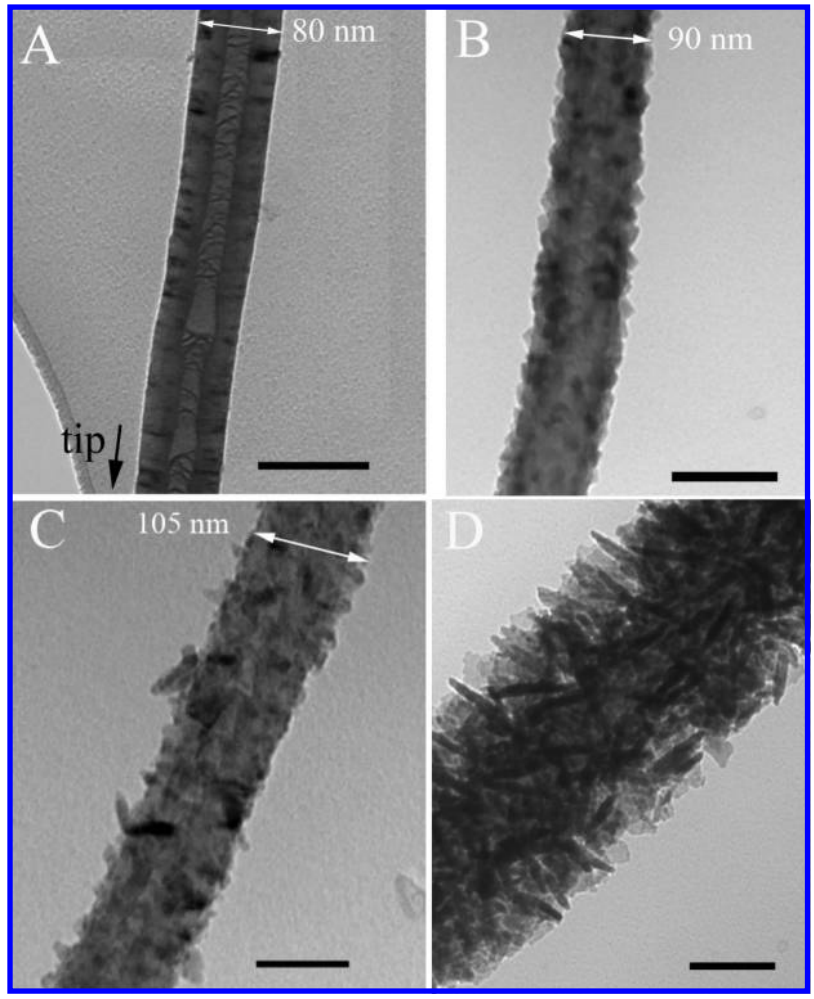

Figure 2. TEM images of (A) an as-grown CNF, and (B), (C), (D) CNFs after coating TiO_2 for 10, 30, and 60 min via MOCVD, respectively. All scale bars are 100 nm.

CNFs, which offer unique advantages for their use as a 3-D template for TiO_2 deposition and dye molecule adsorption. TiO_2 was deposited onto the VACNF array using a MOCVD process at 500−600 °C. Figure 1B−D shows TiO_2 coating on the outerwall of aligned CNFs with increasing thicknesses corresponding to the deposition time of 10, 30, and 60 min. Particulated TiO_2 film conformally wraps around each individual CNFs while they retain the original vertical alignment. The TEM image (Figure 2B) reveals that the TiO_2 layer is 5−10 nm thick after 10 min of deposition. Energy-dispersive X-ray spectroscopy (EDX) measurements on the TiO_2-covered VACNF show strong signals from carbon, titanium, and oxygen (see Figure S2), supporting the TiO_2−CNF core shell composition. Interestingly, a unique nanoneedle-like TiO_2 texture starts to emerge from the initial NPs as the deposition time is increased over 30 min. As shown in Figures 1D and 2D, needle-shaped TiO_2 nanostructure with the mean diameter of 15 nm and the mean length of 50−100 nm was deposited onto the surface of CNF. The orientation of the nanoneedles is random so that most of them tip off from the CNF surface, yielding a large effective surface area.

One important feature is that the TiO_2 NP film or nanoneedles are uniformally deposited along the whole CNFs as shown in Figure 3. The previous study using aligned ZnO NWs as anode in DSCs[5] found that the energy conversion efficiency was limited by the total ZnO surface area, which was only ~1/5 of the TiO_2 NP film. The lack of enough surface area hindered the expected benefits of forming electron speedway in the ZnO NW architecture. The nanoneedle-like texture on the sidewall of VACNFs can overcome this problem by increasing the effective surface area of TiO_2 to the same level of NP films. It would be then very interesting to investigate whether the advantage in collecting electrons through the aligned CNF speedway can be realized.

The crystal structure of the TiO_2 material was characterized by XRD. Figure 4 shows the XRD patterns of TiO_2 nanoneedle coating on VACNFs after 60 min of MOCVD in comparison with a reference sample (a film of commercial TiO_2 NPs of 15 nm in diameter). The diffraction peaks in Figure 4A can be nicely indexed with anatase TiO_2 structure (JCPDS card number 78-2486).[19] The diffraction peak width of the TiO_2−CNF sample is much narrower than the commercial TiO_2 NP, indicating that at least one dimension of the TiO_2 material on CNF is much larger than 15 nm, that is, the diameter of TiO_2 NP. Rocking curve (not shown) indicated that the orientation of the TiO_2 nanoneedle crystals is fully random with a uniform powder pattern. As the deposition time increases, the full-width at half-maximum (fwhm) of (101) diffraction decreases as shown in Figure 4B. The corresponding coherent length of (101) diffraction can be calculated using $L = 2\pi/\Delta q$, where Δq is the fwhm in momentum transfer, giving 11 nm for 10 min of deposition, 19 nm for 30 min of deposition, and 52 nm for 60 min of deposition, respectively. These are consistent with the TEM images shown in Figure 2.

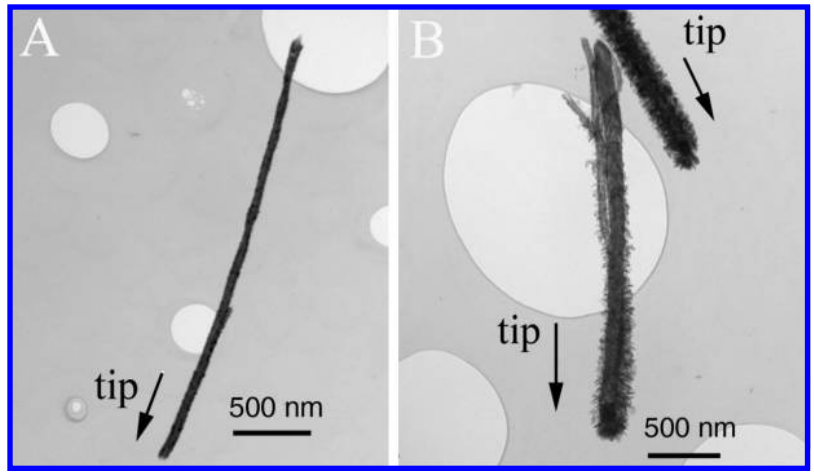

Figure 3. Lower magnification TEM images showing TiO_2 coating covering the whole CNFs after (A) 10 min and (B) 60 min of MOCVD.

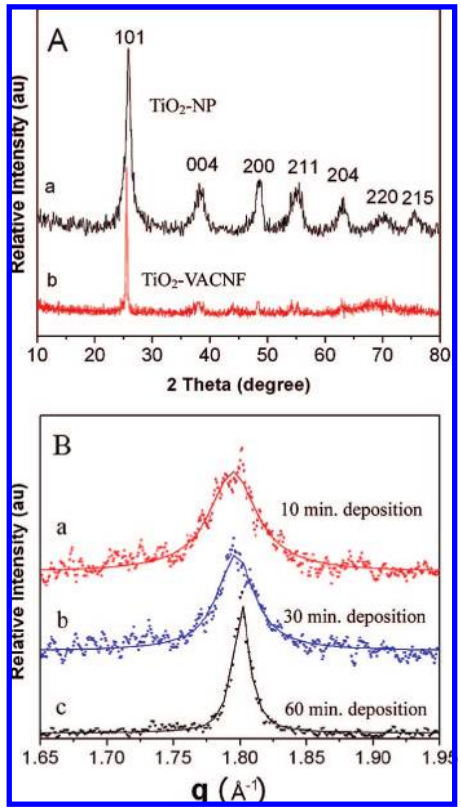

Figure 4. (A) The $\theta-2\theta$ scan of the X-ray diffraction from (a) a film of TiO_2 nanoparticles (15 nm in diam) and (b) the TiO_2 coating on VACNF via 60 min of MOCVD. Both materials can be indexed with anatase TiO_2 crystal structure. (B) The TiO_2 (101) diffraction pattern in momentum transfer $q = 4\pi/\lambda \sin(2\theta/2)$ after (a) 10 min, (b) 30 min, and (c) 60 min of MOCVD, respectively. The data are fit with Lorentzian curves with the full-width at half-maximum at $\Delta q = 0.058$, 0.033, and 0.012 $Å^{-1}$, respectively.

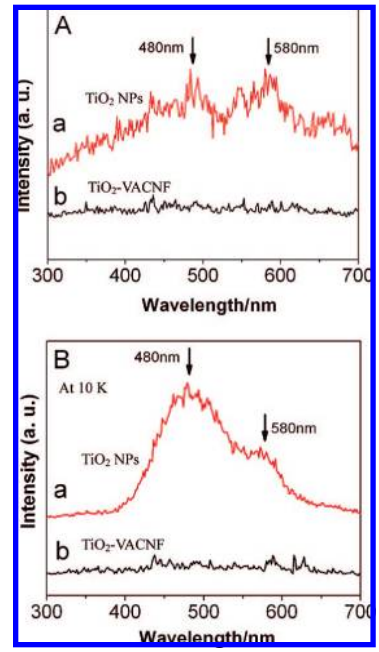

Figure 5. Photoluminescence spectra measured (A) at 300 K and (B) at 10 K. Curve a represents the measurement with a film of TiO_2 nanoparticles (15 nm in diam), and curve b is from the hybrid TiO_2-VACNF array. The excitation wavelength is at 263 nm (4.71 eV).

To investigate the trapping, immigration, and transfer properties of charge carriers, PL spectroscopy measurements have been carried out on the TiO_2-VACNF sample after 60 min of deposition in comparison with a film of commercial TiO_2 NPs (~15 nm in diameter). The PL spectrum of the system is formed as a result of the competition between electron−hole separation, electron−phonon scattering, and electron−hole recombination. TiO_2 has a direct band gap but is subjected to dipole-forbidden transitions.[20] As a result, previous reports demonstrated that it is difficult to observe PL response at room temperature for bulk TiO_2 due to its indirect transition nature.[20,21] However, PL signals were found from TiO_2 NPs[20,23] and thin films.[21,22] Furthermore, the intensity of PL in nanometer-sized TiO_2 increased as the test temperature decreases[24] following the well-known Varshni model.[25] Low-temperature PL measurements can obtain much clearer emissions bands. The band gap energy for anatase TiO_2 crystal is known to be 3.4 eV.[22] Here, the PL spectra were measured with the excitation wavelength at 263 nm (4.71 eV). Figure 5A and B represents PL spectra of TiO_2 NP film and TiO_2-VACNF after 60 min of deposition at 300 and 10 K, respectively. At 300 K (Figure 5A), two characteristic luminescence peaks for TiO_2 NP film are observed at 480 nm (2.58 eV) and 580 nm (2.14 eV) as indicated by the arrows in Figure 5. The PL intensity of both emission bands is significantly enhanced at 10 K with the 480 nm band increasing more than the 580 nm band. No PL band was observed in the region of 300−430 nm (4.13−2.88 eV), which corresponds to band edge luminescence as reported before[23] with liquid-phase prepared anatase TiO_2 NPs. The emission signal at 480 nm can be attributed to the charge-transfer transition from Ti^{3+} to oxygen

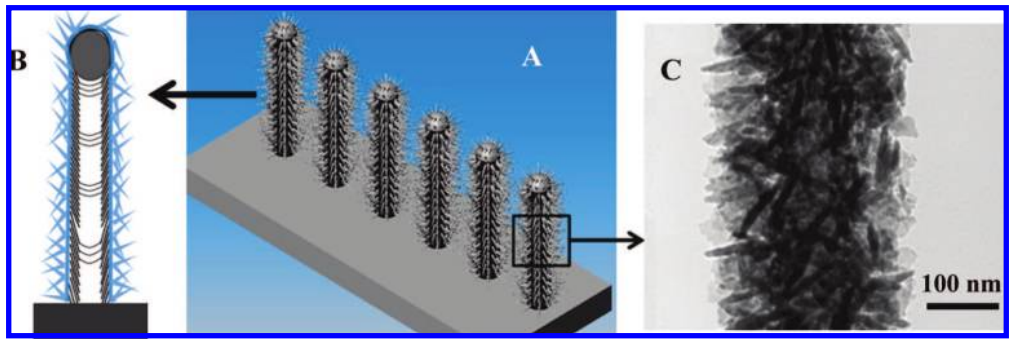

Figure 6. Schematic of the nanoneedle texture on the VACNF array.

anion in a TiO_6^{8-} complex associated with oxygen vacancies at the surface.[26,27] The origin of PL band at 580 nm (2.14 eV), however, is unknown at this moment. At 10 K, most of the excited electrons return to the shallow level, leading to PL enhancement at 480 nm. At room temperature, most electrons in the shallow level are thermally ionized by taking a transition to the conduction band and may recombine through nonradiative transitions, resulting in the rapid decrease in the PL intensity at 480 nm. The intensity reduction with increasing temperature may thus be mainly induced by enhanced nonradiative recombination.[28,29]

Previous studies have shown that room-temperature PL can be obtained by coating the TiO_2 NP surface with stearic acid[20] or −OR groups.[23] For TiO_2 coated on VACNF, we observed the opposite phenomenon. As shown in curve b of Figure 5A and B, the PL bands were completely quenched at both 300 and 10 K. This phenomenon is similar to the results of a recent PL study with various quantum dots (QDs) including CdSe, CdS-coated CdSe, and ZnO, directly attached to MWCNTs.[30] The PL emission bands were recovered after the MWCNT surface was insulated with a thin layer of SiO_2, revealing that MWCNTs were involved in the charge separation. The work functions of MWCNTs[31] and the CNFs in this study are similar (around 4.7−5.0 eV[12,31]). Thus, their Fermi level lies in the gap between the conduction band and valence band of the TiO_2 nanocrystals. The PL quenching may be originated from charge transfer of photoexcited electrons from the conduction band of TiO_2 to the empty electronic states of CNF at the TiO_2−CNF heterojunction, resulting in nonradiative decay of the TiO_2 excited state.[30] This is consistent with the enhanced charge separation observed by Yu et al.[15] in the photoelectrochemical study using TiO_2 NPs on MWCNTs.

It is noteworthy that, even though CNFs share many common properties with MWCNTs, their microstructures are quite different. High-resolution TEM images in our previous study[9] showed that the CNF consisted of a stack of cuplike graphitic cones with the sidewall tilt from the CNF axis, in drastic contrast to the straight concentric tube structure in MWCNTs. This microstructure accounts for the bamboo-like graphitic layers running across the hollow channel at the CNF center. For the same reason, the sidewall of VACNFs also presents many broken graphene edges. The broken edges serve as active sites, which can facilitate the TiO_2 deposition and fast electron transfer.[32] Hence, CNFs are naturally a better template for TiO_2 deposition and more active as an electrode than MWCNTs. This might be the reason that we can obtain the nanoneedle-like TiO_2 texture on CNF surface, while Yu et al.[15] can only obtain a low density of NP film on MWCNT surface. In addition, VACNF array also presents sufficient space between individual CNFs so that a uniform TiO_2 coating can be obtained along the whole CNF from the tip to the bottom. This is a significant improvement from the previous study,[13] which only obtained TiO_2 NP deposition near the tip of MWCNTs.

The previous work by Law et al.[5] has shown great potential for using aligned ZnO NW arrays as electron speedway to improve the performance of DSCs. However, the overall energy conversion efficiency was limited by the fact that even the longest ZnO arrays (with 20−25 μm length and ∼125 aspect ratio)[5,16] had only 1/5 of the active surface area of a traditional 10 μm TiO_2 NP anode.[1,6] The PECVD-grown VACNF array can be easily grown with a density similar to that of ZnO NW arrays and an aspect ratio over 400 (with diameter of ∼50−100 nm and length up to 40 μm). As illustrated in Figure 6, the outer surface of the VACNFs can be further decorated with the nanoneedle texture. The TEM image in Figure 6C shows that the average number of TiO_2 nanoneedles is ∼3.5 in every 100 × 100 nm^2 area. Even using a simple model assuming that the TiO_2 nanoneedles are smooth rods, coating the CNF surface with 15 nm diameter and 100 nm long TiO_2 nanoneedles will increase the surface area by a factor of 3. The roughness of microstructure of the nanoneedles can easily increase the effective surface area by an additional factor of 3−5. The overall effective surface area of the TiO_2−VACNF hierarchical architecture could reach or surpass that of the TiO_2 NP anodes in traditional DSCs.

Conclusions

In summary, we have demonstrated the synthesis of hybrid TiO_2−VACNF architecture by a MOCVD strategy. By tuning the growth time, the structure of TiO_2 can be controlled from a thin NP film to a nanoneedle-like texture. An analysis of the PL spectra indicates complete fluorescence quenching due to electron separation at the heterojunction of TiO_2 and CNFs. Combining the large effective surface area of nanoneedle-like TiO_2 texture with the high intrinsic carrier motilities and fast electron transport through the highly conductive CNF core, this new hierarchical hybrid TiO_2−VACNF architecture may significantly improve the performance of DSCs, photoelectrolysis, photocatalysis, biosensors, and other optoelectronic devices.

Acknowledgment. We would like to thank Dr. Prabhu Arumugam from NASA Ames Research Center for providing some of the VACNF samples. J.L. thanks Kansas State University for financial support.

Supporting Information Available: SEM image of an as-grown VACNF array, energy-dispersive X-ray spectroscopy of a TiO_2-coated VACNF array, and apparent nanofiber diameter. This material is available free of charge via the Internet at http://pubs.acs.org.

References and Notes

(1) Oregan, B.; Gratzel, M. *Nature* **1991**, *353*, 737.
(2) Mor, G. K.; Shankar, K.; Paulose, M.; Varghese, O. K.; Grimes, C. A. *Nano Lett.* **2006**, *6*, 215.
(3) Zhu, K.; Neale, N. R.; Miedaner, A.; Frank, A. J. *Nano Lett.* **2007**, *7*, 69.
(4) Baxter, J. B.; Aydil, E. S. *Appl. Phys. Lett.* **2005**, *86*, 053114.
(5) Law, M.; Greene, L. E.; Johnson, J. C.; Saykally, R.; Yang, P. D. *Nat. Mater.* **2005**, *4*, 455.
(6) Gratzel, M. *Nature* **2001**, *414*, 338–344.
(7) Kind, H.; Yang, H.; Messer, B.; Law, M.; Yang, P. *Adv. Mater.* **2002**, *14*, 158.
(8) Li, J.; Ye, Q.; Cassell, A.; Ng, H. T.; Stevens, R.; Han, J.; Meyyappan, M. *Appl. Phys. Lett.* **2003**, *82*, 2491.
(9) Ngo, Q.; Cassell, A. M.; Austin, A. J.; Li, J.; Krishnan, S.; Meyyappan, M.; Yang, C. Y. *IEEE Electron Device Lett.* **2006**, *27*, 221.
(10) Zhang, L.; Austin, D.; Merkulov, V. I.; Meleshko, A. V.; Klein, K. L.; Guillorn, M. A.; Lowndes, D. H.; Simpson, M. L. *Appl. Phys. Lett.* **2004**, *84*, 3972.
(11) Metz, K. M.; Tse, K. Y.; Baker, S. E.; Landis, E. C.; Hamers, R. J. *Chem. Mater.* **2006**, *18*, 5398.
(12) Gao, R.; Pan, Z.; Wang, Z. L. *Appl. Phys. Lett.* **2001**, *78*, 1757.
(13) Park, Y.; Choong, V.; Gao, Y.; Hsieh, B. R.; Tang, C. W. *Appl. Phys. Lett.* **1996**, *68*, 2699–2701.
(14) Kongkanand, A.; Dominguez, R. M.; Kamat, P. V. *Nano Lett.* **2007**, *7*, 676.
(15) Yu, H. T.; Quan, X.; Chen, S.; Zhao, H. M. *J. Phys. Chem. C* **2007**, *111*, 12987–12991.
(16) Law, M.; Greene, L. E.; Radenovic, A.; Kuykendall, T.; Liphardt, J.; Yang, P. D. *J. Phys. Chem. B* **2006**, *110*, 22652.
(17) Ren, Z. F.; Huang, Z. P.; Xu, J. W.; Wang, J. H.; Bush, P.; Siegal, M. P.; Provencio, P. N. *Science* **1998**, *282*, 1105.
(18) Cruden, B. A.; Cassell, A. M.; Ye, Q.; Meyyappan, M. *J. Appl. Phys.* **2003**, *94*, 4070.
(19) Wu, J. J.; Yu, C. C. *J. Phys. Chem. B* **2004**, *108*, 3377–3379.
(20) Zou, B.; Xiao, L.; Li, T.; Zhao, J.; Lai, Z.; Gu, S. *Appl. Phys. Lett.* **1991**, *59*, 1826.
(21) Bai, N.; Li, S. G.; Chen, H. Y.; Pang, W. Q. *J. Mater. Chem.* **2001**, *11*, 3099.
(22) Yu, J. G.; Yu, H. G.; Cheng, B.; Zhao, X. J.; Yu, J. C.; HO, W. K. *J. Phys. Chem. B* **2003**, *107*, 13871.
(23) Abazovic, N. D.; Comor, M. I.; Dramicanin, M. D.; Jovanovic, D. J.; Ahrenkiel, S. P.; Nedeljkovic, J. M. *J. Phys. Chem. B* **2006**, *110*, 25366–25370.
(24) Melnyk, V.; Shymanovska, V.; Puchkovska, G.; Bezrodna, T.; Klishevich, G. *J. Mol. Struct.* **2005**, *573*, 744–747.
(25) Varshni, Y. P. *Physica* **1967**, *34*, 149.
(26) Yu, J. C.; Yu, J. G.; Ho, W. K.; Zhang, L. Z. *Chem. Mater.* **2002**, *14*, 3808.
(27) Li, F. B.; Li, X. Z. *Chemosphere* **2002**, *48*, 1103.
(28) Mintairov, A. M.; Kosel, T. H.; Merz, J. L.; Blagnov, P. A.; Vlasov, A. S.; Ustinov, V. M.; Cook, R. E. *Phys. Rev. Lett.* **2001**, *87*, 277401.
(29) Luo, S. H.; Fan, J. Y.; Liu, W. L.; Zhang, M.; Song, Z. T.; Lin, C. L.; Wu, X. L.; Chu, P. K. *Nanotechnology* **2006**, *17*, 1695.
(30) Olek, M.; Busgen, T.; Hilgendorff, M.; Giersig, M. *J. Phys. Chem. B* **2006**, *110*, 12901–12904.
(31) Liu, P.; Sun, Q.; Zhu, F.; Liu, K.; Jiang, K.; Liu, L.; Li, Q.; Fan, S. *Nano Lett.* **2008**, *8*, 647–651.
(32) Koehne, J.; Li, J.; Cassell, A. M.; Chen, H.; Ye, Q.; Ng, H. T.; Han, J.; Meyyappan, M. *J. Mater. Chem.* **2004**, *14*, 676–684.

JP8060653